Assembly of High-Areal-Density Deuterium-Tritium Fuel from Indirectly Driven Cryogenic Implosions

A. J. Mackinnon,[1] J. L. Kline,[3] S. N. Dixit,[1] S. H. Glenzer,[1] M. J. Edwards,[1] D. A. Callahan,[1] N. B. Meezan,[1] S. W. Haan,[1] J. D. Kilkenny,[5] T. Döppner,[1] D. R. Farley,[1] J. D. Moody,[1] J. E. Ralph,[1] B. J. MacGowan,[1] O. L. Landen,[1] H. F. Robey,[1] T. R. Boehly,[2] P. M. Celliers,[1] J. H. Eggert,[1] K. Krauter,[1] G. Frieders,[1] G. F. Ross,[1] D. G. Hicks,[1] R. E. Olson,[4] S. V. Weber,[1] B. K. Spears,[1] J. D. Salmonsen,[1] P. Michel,[1] L. Divol,[1] B. Hammel,[1] C. A. Thomas,[1] D. S. Clark,[1] O. S. Jones,[1] P. T. Springer,[1] C. J. Cerjan,[1] G. W. Collins,[1] V. Y. Glebov,[2] J. P. Knauer,[2] C. Sangster,[2] C. Stoeckl,[2] P. McKenty,[2] J. M. McNaney,[1] R. J. Leeper,[4] C. L. Ruiz,[4] G. W. Cooper,[8] A. G. Nelson,[8] G. G. A. Chandler,[4] K. D. Hahn,[4] M. J. Moran,[1] M. B. Schneider,[1] N. E. Palmer,[1] R. M. Bionta,[1] E. P. Hartouni,[1] S. LePape,[1] P. K. Patel,[1] N. Izumi,[1] R. Tommasini,[1] E. J. Bond,[1] J. A. Caggiano,[1] R. Hatarik,[1] G. P. Grim,[3] F. E. Merrill,[3] D. N. Fittinghoff,[1] N. Guler,[3] O. Drury,[1] D. C. Wilson,[3] H. W. Herrmann,[3] W. Stoeffl,[1] D. T. Casey,[6] M. G. Johnson,[6] J. A. Frenje,[6] R. D. Petrasso,[6] A. Zylestra,[6] H. Rinderknecht,[6] D. H. Kalantar,[1] J. M. Dzenitis,[1] P. Di Nicola,[1] D. C. Eder,[1] W. H. Courdin,[1] G. Gururangan,[1] S. C. Burkhart,[1] S. Friedrich,[1] D. L. Blueuel,[1] l. A. Bernstein,[1] M. J. Eckart,[1] D. H. Munro,[1] S. P. Hatchett,[1] A. G. Macphee,[1] D. H. Edgell,[2] D. K. Bradley,[1] P. M. Bell,[1] S. M. Glenn,[1] N. Simanovskaia,[1] M. A. Barrios,[1] R. Benedetti,[1] G. A. Kyrala,[3] R. P. J. Town,[1] E. L. Dewald,[1] J. L. Milovich,[1] K. Widmann,[1] A. S. Moore,[7] G. LaCaille,[1] S. P. Regan,[2] L. J. Suter,[1] B. Felker,[1] R. C. Ashabranner,[1] M. C. Jackson,[1] R. Prasad,[1] M. J. Richardson,[1] T. R. Kohut,[1] P. S. Datte,[1] G. W. Krauter,[1] J. J. Klingman,[1] R. F. Burr,[1] T. A. Land,[1] M. R. Hermann,[1] D. A. Latray,[1] R. L. Saunders,[1] S. Weaver,[1] S. J. Cohen,[1] L. Berzins,[1] S. G. Brass,[1] E. S. Palma,[1] R. R. Lowe-Webb,[1] G. N. McHalle,[1] P. A. Arnold,[1] L. J. Lagin,[1] C. D. Marshall,[1] G. K. Brunton,[1] D. G. Mathisen,[1] R. D. Wood,[1] J. R. Cox,[1] R. B. Ehrlich,[1] K. M. Knittel,[1] M. W. Bowers,[1] R. A. Zacharias,[1] B. K. Young,[1] J. P. Holder,[1] J. R. Kimbrough,[1] T. Ma,[1] K. N. La Fortune,[1] C. C. Widmayer,[1] M. J. Shaw,[1] G. V. Erbert,[1] K. S. Jancaitis,[1] J. M. DiNicola,[1] C. Orth,[1] G. Heestand,[1] R. Kirkwood,[1] C. Haynam,[1] P. J. Wegner,[1] P. K. Whitman,[1] A. Hamza,[1] E. G. Dzenitis,[1] R. J. Wallace,[1] S. D. Bhandarkar,[1] T. G. Parham,[1] R. Dylla-Spears,[1] E. R. Mapoles,[1] B. J. Kozioziemski,[1] J. D. Sater,[1] C. F. Walters,[1] B. J. Haid,[1] J. Fair,[1] A. Nikroo,[5] E. Giraldez,[5] K. Moreno,[5] B. Vanwonterghem,[1] R. L. Kauffman,[1] S. Batha,[3] D. W. Larson,[1] R. J. Fortner,[1] D. H. Schneider,[1] J. D. Lindl,[1] R. W. Patterson,[1] L. J. Atherton,[1] and E. I. Moses[1]

[1]*Lawrence Livermore National Laboratory, Livermore, California 94551, USA*
[2]*Laboratory for Laser Energetics, University of Rochester, Rochester, New York 14623, USA*
[3]*Los Alamos National Laboratory, Los Alamos, New Mexico, 87545, USA*
[4]*Sandia National Laboratory, New Mexico 87123, USA*
[5]*General Atomics, General Atomics, San Diego, California 92186, USA*
[6]*Plasma Science and Fusion Center, Massachusetts Institute of Technology, Cambridge, Massachusetts 02139, USA*
[7]*AWE, Aldermaston, Reading, Berkshire, RG7 4PR, United Kingdom*
[8]*Chemical and Nuclear Engineering Department, University of New Mexico, Albuquerque, New Mexico 87131*

(Received 18 December 2011; published 24 May 2012)

The National Ignition Facility has been used to compress deuterium-tritium to an average areal density of $\sim 1.0 \pm 0.1$ g cm^{-2}, which is 67% of the ignition requirement. These conditions were obtained using 192 laser beams with total energy of 1–1.6 MJ and peak power up to 420 TW to create a hohlraum drive with a shaped power profile, peaking at a soft x-ray radiation temperature of 275–300 eV. This pulse delivered a series of shocks that compressed a capsule containing cryogenic deuterium-tritium to a radius of 25–35 μm. Neutron images of the implosion were used to estimate a fuel density of 500–800 g cm^{-3}.

DOI: 10.1103/PhysRevLett.108.215005 PACS numbers: 52.57.−z, 52.38.−r, 52.50.−b

In indirect-drive inertial confinement fusion, laser energy is converted to thermal x rays inside a high-Z cavity (hohlraum) [1]. These x rays then ablate the outer layers of a cryogenically layered deuterium-tritium (DT) filled low-Z capsule placed at the center of the hohlraum, causing the capsule to implode, compressing and heating the deuterium and tritium ions. To achieve fusion ignition, the plasma density and temperature must be maintained to initiate a self propagating burn wave before disassembly or cooling reduces the fusion reaction rate and hence fusion power gain below the power losses of radiation and thermal conduction. To efficiently burn a significant fraction of the DT fuel, areal densities (ρR) larger than 1 g cm^{-2} are required [1,2]. Previously the highest ρR (0.295 ± 0.044 g cm^{-2}) was measured in direct drive experiments on the Omega laser at the University of Rochester [3]. These experiments used a laser pulse shape that was tuned to produce a low adiabat implosion (where the in-flight (IF)

adiabat, α_{IF} is defined as the ratio of fuel pressure to Fermi pressure at the fuel density).

A strategy to achieve high-ρR implosions using indirectly driven capsules on the National Ignition Facility (NIF) [4] is described in a series of articles by Landen, Haan, Edwards *et al.*, [5–7]. This methodology requires experiments to optimize implosion symmetry [8], laser-hohlraum coupling [9], and accurate timing of the shocks that drive the implosion [10,11]. The point design for these implosions defines a laser pulse containing four distinct intensity steps in time, which create a temporal x-ray flux profile, tailored to compress the capsule via 3 shocks, which are followed by quasiadiabatic compression around the peak of the drive [6]. When the strength and timing of these shocks is properly adjusted the capsule is designed to have $\alpha_{IF} < 1.5$. To achieve low α_{IF} the shocks need to merge close to the inner DT solid-fuel–gas interface. Significant deviations from the designed shock strength and/or timing leads to shock merger either within the ice layer or too far into the central gas region, which can lead to preheat and reduction of ρR at peak compression [3,6].

Optimal shock timing is achieved using a capsule filled with cryogenic liquid deuterium as a surrogate for the cryogenic solid DT fuel layer [10,11]. This technique allows tuning of the laser pulse to achieve optimal shock strengths and merger depths in solid DT ice. A detailed description of the shock tuning experiments that defined the pulse shape used in these experiments is described by H. Robey *et al.* [12],

This Letter describes a series of experiments at the NIF that investigated the implosion conditions created using a shock-tuned laser pulse. The compressibility of the imploded assembly was inferred from measurements of the ratio of down-scattered (10–12 MeV) neutrons to primary (13–15 MeV) neutrons. This down-scattered ratio (DSR), is proportional to the areal density "ρR" of the fuel surrounding the neutron producing plasma [13]. For a point source of neutrons surrounded by fuel with areal density ρR (in units of g cm^{-2}), DSR $= \sigma_{DS}\rho R$ where σ_{DS} is the elastic scattering cross section for the fuel; for DT, $\sigma_{DS} = 0.045$ cm^2 g^{-1} and fuel $\rho R = 1$ g cm^{-2} would give DSR $= 0.045$. The spatial characteristics of the stagnating plasma were obtained from gated x-ray imaging of >6 keV x rays [8] and time integrated images [14] of primary and down-scattered neutrons.

The experimental geometry used to drive these implosions has been described in detail by Glenzer *et al.* [9]. To summarize: 192 laser beams at nominal wavelength of 351 nm, total energy of 1.0–1.6 MJ are focused in two cones through the laser entrance holes of the hohlraum. The x-ray drive delivered by these pulses gave a peak radiation temperature of 275–300 eV, with peak soft x-ray flux of 11–15.7 TW/cm^2 by the end of a 20 ns pulse [9]. The x-ray drive was incident on spherical capsules with an outer radius $= 1.12$ mm $\pm$ 15 μm, and with 193 $\pm$ 5 μm thick ablator, consisting of multilayered plastic (CH) with a graded germanium or silicon dopant, surrounding a layer of solid (equi-molar) DT. The ablator is designed to absorb thermal x rays from the hohlraum while preventing higher energy x rays from preheating the inside of the ablator to avoid a hydrodynamically unstable density differential between ablator and fuel [6]. The DT fuel forms a spherical ice layer on the inner surface of the ablator with a nominal thickness of 69 $\pm$ 1 μm. The central cavity of the capsule contains DT vapor in equilibrium with the ice layer. The uniformity of the ice is maintained via energy deposition from spontaneous beta decay from tritium atoms in the layer [15]. To reduce the neutron yield in some of these experiments the relative concentration of deuterium in some capsules was reduced (as neutron yield is proportional to the product of deuteron and tritium ions) from 50% to 6% by replacement of deuterium by hydrogen. These "tritium-hydrogen-deuterium" capsules allowed optimum signal levels for the neutron diagnostics while maintaining adequate signal to neutron background for the x-ray imaging diagnostics [7].

A series of shock tuning experiments prior to the implosion experiments determined that adjustments of 10%–20% were required for the laser power levels in shocks 1–3 and resulted in a pulse 800 ps longer than the pretuned case [12]. The x-ray drive from the shock-tuned laser pulse was predicted to produce a low adiabat implosion with $\alpha_{IF} \sim 1.7 - 1.5$, and fuel $\rho R \sim 1.2$–1.4 g cm^{-2} (DSR $= 0.05$–0.6), approaching the ignition requirement, $\alpha_{IF} \sim 1.46$; $\rho R \sim 1.5$–1.7 g cm^{-2} (DSR $= 0.07$) [6].

The performance of indirect implosions driven by these pulses was diagnosed using a suite of x-ray and nuclear diagnostics [7]. The spatially averaged DSR for the implosions was obtained using the magnetic recoil spectrometer (MRS) [13] and three high dynamic range neutron time of flight (NTOF) detectors [16], giving four different viewing angles to the imploded capsule. The MRS uses a 50–250 μm CD foil in which escaping MeV neutrons create forward knock-on MeV deuterons that can be energy resolved using a magnet and solid-state track detectors. Because the CD foil is thin (~ 250 μm) the deuteron spectrum can be used to deduce the incident neutron spectrum with high fidelity [17]. The MRS system is an established technique that has been used extensively to characterize the DSR (ρR) in direct drive cryogenic DT implosions on the Omega laser [3,17]. The NTOF array of photoconductive detectors and scintillator/photomultiplier systems at 4.5 to 20 m measures the arrival time of the neutrons generated during the implosion, to extract ion temperature T_{ion} *via* temporal broadening of the 13–15 MeV neutron pulse and the relative ratio of down-scattered neutrons to the 13–15 MeV neutron signal [16]. All these instruments also measure the absolute yields.

Example MRS spectra for shots before and after shock tuning are shown in Fig. 1. The diagnostic setup was

identical for the two shots, allowing a direct comparison of the deuteron spectra. The pretuning example [experiment N110212 with a fuel mixture of T(74%):D(6%):H(20%)] gave a primary neutron yield $Y_n = 1.2e14 \pm 5\%$, $T_{\text{ion}} = 3.6$ keV $\pm$ 7%. The post-tuning example [experiment N110608 with a fuel mixture of T(50%):D(50%)] gave $Y_n = 1.93e14 \pm 5\%$, $T_{\text{ion}} = 3.1$ keV $\pm$ 7%. The unscattered neutrons produce the broad peak centered at 11.5 MeV, while the down-scattered neutrons are responsible for the signal between 7 and 10 MeV. The plots have been normalized by their 13–15 MeV neutron yields to show the increase in DSR in the post-tuned vs the pretuned case, as observed in Fig. 1. Analysis of these data gave $\text{DSR}_{\text{MRS}} = 0.027 \pm 0.003$ for pretuned and $\text{DSR}_{\text{MRS}} = 0.043 \pm 0.003$ ($\rho R \sim 0.90$ g cm^{-2}) for post tuned, a factor of 1.6 increase from shock tuning. The spatially averaged DSR_{mean} was obtained for each implosion from a weighted mean of the MRS measured DSR and the three NTOF diagnostics.

Figure 2 summarizes DSR_{MRS} and DSR_{mean} results for this series of experiments. Four experiments carried out before shock tuning generated assembled fuel with DSR_{mean} within the range of 0.025 to 0.028. Of the eight experiments carried out after shock tuning, seven produced DSR_{mean} within range 0.04 to 0.049. This represented a stepwise increase of $\sim$1.6$\times$ in the observed DSR_{mean} as a result of the shock tuning.

The implosion experiments were modeled using the HYDRA 2D simulation code [18]. The x-ray source drive in the simulations was varied until it matched the shock velocity history observed [12] for the first 19 ns up to peak power and then matched the implosion trajectory measured via x-ray radiography [19]. The implosion symmetry was also matched using the plasma cross-beam transfer saturation parameter that determines the relative balance of inner and outer laser beam power [20]. This parameter was empirically set from the observed symmetry on the first post-tuned tritium-hydrogen-deuterium experiment (N110603). Realistic levels of capsule ablator and ice surface roughness were also included for modes up to 60, since these are predicted by the point design to have the highest Rayleigh-Taylor instability growth rate [6]. When the measured capsule and ice roughness was applied to all the surfaces and interfaces in the calculation, significant Rayleigh-Taylor growth was seen at the ice–gas interface compared to 2D clean calculations, cooling the hotspot, lowering neutron yield, ρR, and DSR. This model was used to infer implosion observables, including neutron spectrum (13–15 MeV), neutron yield, DSR, ion temperature, gamma ray emission, time/space resolved x-ray and neutron emission from the imploded capsule. These HYDRA "mode 60" simulations included corrections to the drive caused by deviations from requested laser pulse shapes and variations in target dimensions [21].

The simulated DSR from the mode 60 simulations for the shock-tuned implosions are within 25% of the measured DSR, as shown in Fig. 2. The in-flight adiabat inferred from these simulations ranged from 1.5 to 1.73. The simulations matched the observed ion temperature to within 20% and the ratio of experimentally measured yield over simulated was in the range of 10%–45% for the 8 shock-timed implosions.

X-ray imaging above 6 keV allows a direct determination of the hot spot (HS) radius, R_{HS}, at stagnation; this is a key parameter that should be strongly correlated with the ρR achieved by the implosion [6,7]. When properly tuned these implosions are designed to achieve $R_{\text{HS}} = 25$–30 μm. Shock mistiming can lead to rarefaction at the DT ice-vapor interface reducing compressibility, resulting in a larger observed R_{HS}. Pinhole imaging coupled to a gated microchannel plate, with spatial and temporal resolution of 7 μm and 40–50 ps, respectively, was used to record hot spot x-ray emission >6 keV [22]. Two systems provided orthogonal views of hot spot x-ray emission from

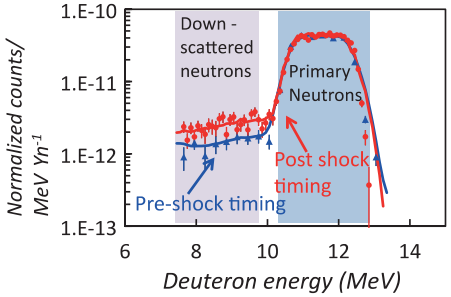

FIG. 1 (color). MRS data from two experiments; N110212 (preshock timing–blue points and line) and N110608 (post-shock timing–red points and line). The data have been normalized to 13–15 MeV neutron yield to allow direct comparison. Data were taken with the same MRS foil thickness and normalized to 13–15 MeV neutron yield.

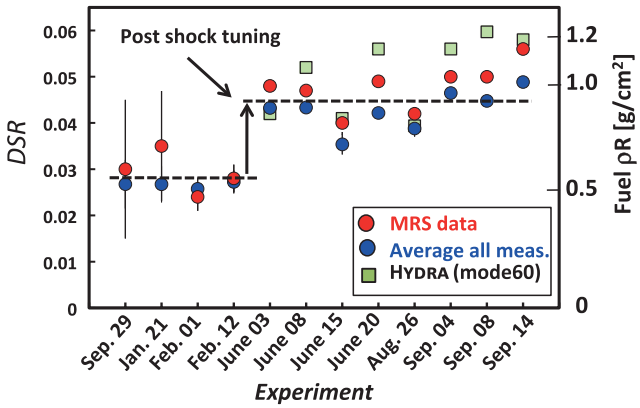

FIG. 2 (color). DSR as measured by MRS (red points) and average of all down-scatter detectors (blue points) vs experiment date. The green boxes are DSR from 2D HYDRA mode 60 simulations with radiation asymmetry, measured capsule and ice roughness and drive adjusted to match the observed shock-timing results, as described in the text.

the pole through the laser entrance holes and on the equator through a diagnostic patch in the hohlraum wall [8]. R_{HS} is defined as the 17% contour of the x-ray emission based on simulations with little mixing of fuel and hot spot.

A complementary measurement of both hot spot and fuel size was obtained from a neutron pinhole imaging system [14]. It utilizes a scintillator and two gated CCD cameras designed to obtain time integrated pinhole images of the 13–17 MeV neutrons emitted from the hot spot and 10–12 MeV neutrons down scattered from the cold fuel. Both x-ray and neutron emission imaging were used to investigate correlations between measured DSR and R_{HS}.

Before shock tuning, gated x-ray images of the hot spot at the time of peak x-ray emission were large with $R_{HS} =$ 40–45 μm. In contrast the x-ray images post shock-timing display significantly reduced R_{HS} with radii in the range of 22–35 μm. These data are consistent with an improvement in compressibility and fuel density. From a simple 1D shell model, where all the fuel mass, M_{fuel} is located in an annular region of thickness Δr at radius R_{HS}, giving $\rho\Delta r = \mathrm{DSR}/\sigma_{ds} = M_{fuel}/4\pi R_{HS}^2$. Improved areal density correlates to smaller hot spot area, radius. On average the observed equatorial hot spot area reduced by a factor of 1.8 ± 0.3 after shock tuning while the DSR increased by a factor of 1.6 ± 0.2, in reasonable agreement with this 1D shell model.

To further examine performance, a plot of DSR vs $1/R_{HS}^2$, is shown in Fig. 3. Here $1/R_{HS}^2$ inferred from the gated x-ray and time integrated neutron images are both shown (neutron images of the R_{HS} agreed to within 10% to the gated x-ray measurements). As the DSR increases the hot spot area reduces, approximately in line with the 1D model. We can go beyond a shell approximation by expressing the fuel mass and density in terms of the volume of the shell, $M_{fuel} = \rho_{fuel} 4/3\pi\ [(R_{HS} + \Delta r)^3 - R_{HS}^3]$ as shown in Fig. 3, where R_{HS} is now related to the inside edge of the fuel. A straight line on the DSR vs $1/R_{HS}^2$ plot has slope $= \mathrm{DSR}/(1/R_{HS}^2) = M_{fuel}[4\pi(1 + \Delta r/R_{HS} + \Delta r^2/3R_{HS}^2)]^{-1}$. In the limit of thin shells and/or large hot spots, $\Delta r/R_{HS} \to 0$ and the slope $= M_{fuel}/4\pi$. As the hot spot reduces and/or shell thickens, $\Delta r/R_{HS}$ increases, and the slope reduces. This is shown on Fig. 3 with the lines representing $\Delta r/R_{HS} = 0$, 0.5, 0.7, and 1.3. HYDRA 2D mode 60 simulations follow $\Delta r/R_{HS} = 0.7$ while the experimental data from x-ray and neutron imaging is more scattered, falling between $\Delta r/R_{HS} = 0.1$ and 1.

The variability in R_{HS} for given DSR may be due in part to cold fuel or ablator material mixing into the gas. This would change the location of the observed x-ray and neutron-emitting hot spot edge so that it does not necessarily correspond to the start of the high density fuel region. Variations in the ice roughness could be a source of this shot to shot variability, though ablator roughness and deviations from symmetry also play a role in determining R_{HS}. More direct investigation of mixing is

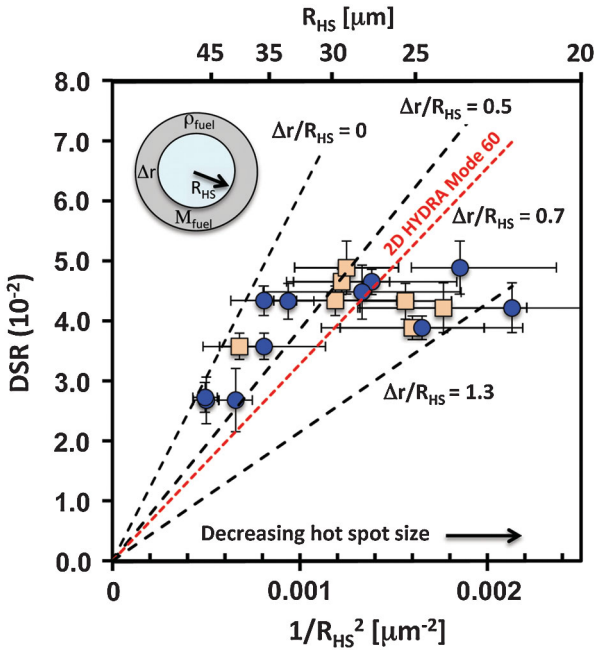

FIG. 3 (color). Plot of DSR vs $1/R_{HS}^2$ determined from gated x-ray images at energies > 6 keV (blue points), time integrated neutron images at 13–15 MeV (tan squares) and 2D HYDRA mode 60 simulations (red dashed line). Also shown is a schematic of uniform shell model with fuel layer of thickness Δr outside hot spot radius, R_{HS}. The lines represent the expected dependence for various assumed values of $\Delta r/R_{HS}$.

planned for future experiments. These will involve spectroscopic measurements from germanium and copper dopants in the ablator [23]. If these dopants are mixed into the hot spot they emit K-shell line radiation that can be used to estimate the amount of ablator material in the hot spot.

Both 13–17 MeV and 10–12 MeV neutron images were obtained from a subset of these implosions. An estimate of the fuel shell thickness Δr can be obtained from these data by again assuming a 1D shell model and subtracting the primary image from the down-scattered image [14]. For experiment N110914: $\Delta r = R_{[10-12]} - R_{HS} =$ $41 - 27\ \mu\mathrm{m} = 14 \pm 3\ \mu\mathrm{m}$, giving $\Delta r/R_{HS} = 0.5$, close to the value of 0.52 inferred from the measured DSR and R_{HS} for this experiment. This measurement also implies $\rho_{fuel} \sim 500$–$800\ \mathrm{g\,cm^{-3}}$ from a $\rho_{fuel}\Delta r \sim 1.0\ \mathrm{g\,cm^{-2}}$ (using measured DSR = 0.049 and 1D shell model).

The performance of the pre and post-tuned pulses are summarized in Fig. 4, which shows measured neutron yield (normalized to the equivalent yield of equimolar DT to account for different fractions of deuterium for the different shots in the series) vs DSR. An implosion metric called the experimental ignition threshold factor, $\mathrm{ITF_{expt}} = (Y_n/3.2e15)(\mathrm{DSR}/0.07)^{2.3}$ is also plotted in Fig. 4. This is a form of the generalized Lawson criteria for inertial confinement fusion [6,7,24] and is a measure of implosion performance (by definition for $\mathrm{ITF_{expt}} = 1$,

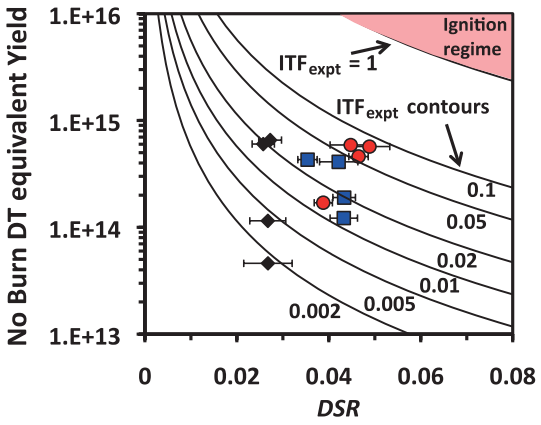

FIG. 4 (color). Plot of DT equivalent yield vs DSR for pretuned (black) and post-tuned pulses with germanium doped (blue) and silicon doped (red) CH ablators. Also shown are contours of equal ITF$_{expt}$, which increase from left to right as yield and DSR increase.

probability of ignition = 0.5). Implosions with shock-tuned pulses produced roughly equivalent yields to pretuned, but with significantly improved DSR, resulting in an ITF$_{expt}$ increase from 0.02 to 0.09. Thus, shock timing led to an increase of 4 in the integrated implosion performance. Further increase in ITF$_{expt}$ will require further improvement to shock timing to achieve $\rho r > 1.5$ g cm^{-2}, increasing the implosion velocity and optimizing the implosion symmetry to increase neutron yields.

In summary indirect-drive implosion experiments have been carried out on the National Ignition Facility using shock-timed pulses. Down-scattered neutron spectra were consistent with a DSR of 0.044 ± 0.0015 ($\rho R \sim 0.97 \pm 0.03$ g cm^{-2}) for shock-timed pulses, compared to a DSR of 0.027 ± 0.002 ($\rho R \sim 0.5$ g cm^{-2}) for pretuned pulses. These results were consistent with observed improvements in capsule compressibility, via x-ray and neutron imaging and with 2D simulations including mix. Further work is underway to improve both the neutron yield and fuel density, to increase the ITF$_{expt}$ closer to ignition conditions.

We wish to thank the NIF operations team without whom these experiments would not have been possible. This work was performed under the auspices of the Lawrence Livermore National Security, LLC, (LLNS) under Contract No. DE-AC52-07NA27344.

[1] J. D. Lindl, Phys. Plasmas **2**, 3933 (1995).
[2] S. Atzeni and J. Meyer-Ter-Vehn, *The Physics of Inertial Confinement Fusion* (Clarendon, Oxford, 2004).
[3] V. Goncharov *et al.*, Phys. Rev. Lett. **104**, 165001 (2010).
[4] G. H. Miller, E. I. Moses, and C. R. Wuest, Nucl. Fusion **44**, S228 (2004).
[5] O. Landen *et al.*, Phys. Plasmas **18**, 051002 (2011).
[6] S. W. Haan *et al.*, Phys. Plasmas **18**, 051001 (2011).
[7] M. J. Edwards *et al.*, Phys. Plasmas **18**, 051003 (2011).
[8] P. Michel *et al.*, Phys. Rev. Lett. **102**, 025004 (2009); G. Kyrala *et al.*, Phys. Plasmas **18**, 056307 (2011).
[9] S. H. Glenzer *et al.*, Phys. Rev. Lett. **106**, 085004 (2011).
[10] T. R. Boehly, V. N. Goncharov, W. Seka, M. A. Barrios, P. M. Celliers, D. G. Hicks, G. W. Collins, S. X. Hu, J. A. Marozas, and D. D. Meyerhofer, Phys. Rev. Lett. **106**, 195005 (2011); T. R. Boehly, Phys. Plasmas **16**, 056302 (2009);
[11] H. F. Robey *et al.*, Phys. Plasmas **19**, 042706 (2012).
[12] H. F. Robey *et al.*, preceding Letter, Phys. Rev. Lett. **108**, 215004 (2012).
[13] J. A. Frenje *et al.*, Rev. Sci. Instrum. **79**, 10E502 (2008).
[14] D. C. Wilson, W. C. Mead, L. Disdier, M. Houry, J.-L. Bourgade, T. J. Murphy, Nucl. Instrum. Methods Phys. Res., Sect. A **488**, 400 (2002); G. Grim *et al.*, J. Phys. IV (Colloque) **133**, 913 (2006); M. D. Wilke *et al.*, Rev. Sci. Instrum. **79**, 10E529 (2008).
[15] A. J. Martin, R. J. Simms, and R. B. Jacobs, J. Vac. Sci. Technol. A **6**, 1885 (1988); B. J. Kozioziemski, E. R. Mapoles, J. D. Sater, A. A. Chernov, J. D. Moody, J. B. Lugten, and M. A. Johnson, Fusion Sci. Technol. **59**, 14 (2011).
[16] V. Y. Glebov *et al.*, Rev. Sci. Instrum. **81**, 10D325 (2010); V. Y. Glebov *et al.*, Rev. Sci. Instrum. **77**, 10E715 (2006).
[17] J. A. Frenje *et al.*, Phys. Plasmas **17**, 056311 (2010).
[18] M. Marinak, G. D. Kerbel, N. A. Gentile, O. Jones, D. Munro, S. Pollaine, T. R. Dittrich, and S. W. Haan, Phys. Plasmas **8**, 2275 (2001).
[19] D. Hicks, B. K. Spears, D. G. Braun, R. E. Olson, C. M. Sorce, P. M. Celliers, G. W. Collins, and O. L. Landen, Phys. Plasmas **17**, 102703 (2010).
[20] P. Michel *et al.*, Phys. Plasmas **17**, 056305 (2010).
[21] O. Jones *et al.*, Phys. Plasmas (to be published).
[22] N. Izumi *et al.*, Inst. Phys. Conf. Ser. **244**, 032048 (2010); J. A. Oertel *et al.*, Rev. Sci. Instrum. **77**, 10E308 (2006).
[23] B. Hammel *et al.*, Phys. Plasmas **18**, 056310 (2011); S. P. Regan *et al.*, Eur. J. Phys. (to be published).
[24] C. D. Zhou and R. Betti, Phys. Plasmas **15**, 102707 (2008).